2022 9th IEEE RAS/EMBS International Conference for Biomedical Robotics and Biomechatronics (BioRob) | 978-1-6654-5849-8/22/$31.00 ©2022 IEEE | DOI: 10.1109/BIOROB52689.2022.9925478

A Multi-Body Model of an upper-limb prosthesis for grip force estimation and related object interaction application

Giulia Bruni[1], Anna Bucchieri[1], Federico Tessari, Nicolò Boccardo, Andrea Marinelli, Student Member, IEEE, Elena De Momi, Memebr, IEEE, Matteo Laffranchi, Member, IEEE, Lorenzo De Michieli, Member, IEEE

***Abstract*— Hand amputation greatly affects the ability of a person to perform activities of daily living (ADLs). For this reason, prosthetic hands should present grasping characteristics to allow the manipulation of objects of different shapes and dimensions. This is the case of the Hannes prosthetic hand, an under-actuated myoelectric prosthesis able to adapt the grasping configuration to the object shape using the actuation of a single motor and the differential mechanism that characterize this device. In this paper, we present the development of a multi-body and multi-domain model of the Hannes hand, which was experimentally validated using an external grasp force sensor to compare the model outcomes to the actual results. The model is used to investigate the correlation between available measurements from the prosthesis and the stiffness of the grasped objects, passing by the exploration of one of the most challenging aspects for tendon-driven under-actuated prosthetic devices: the friction experienced in the transmission mechanism. Therefore, the current analysis leads to the development of a novel control strategy through the use of an object stiffness classifier. The work provides an alternative model-based approach to overcome the absence of force sensors in under-actuated prosthetic hands for object recognition tasks. The obtained results are promising with contained percentage errors.**

I. INTRODUCTION

Recent technological developments have introduced poly-articulated prosthetic hands with the aim of providing devices capable to reproduce human-like grasping behaviours, such as the Vanderbilt Multigrasp Hand [1], the Hannes Hand [2], the SoftHand Pro [3] and the MIA hand [4]. Nevertheless, there is still a relevant gap between amputee desires and what a prosthetic system can offer to the patient. For this reason, the majority of unilateral amputees prefers to use the healthy limb to perform most of their activities of daily living (ADLs) [5]. Upper-limb prostheses are also characterized by high rate of abandonment due to the unfulfillment of two of the most required demands, namely human-like grasps and a haptic feedback related to the characteristics of the grasped object [6]–[10]. To satisfy the first requirement, multi degrees of freedom (DoFs) under-actuated prostheses were introduced [11]. These systems present fewer motor units with respect to the available DoFs leading to light weight, power efficiency, and cost effectiveness [12], [13]. When using a myoelectric prothesis, the lack of a haptic feedback reduces the feeling of connection with the non-physiological hand and brings the subject not to be engaged in active grasping and exploration [14]. Different studies propose the implementation of a tactile sensation by employing force sensors coupled with vibrating units [14]–[17]. However, this approach presents several drawbacks such as bulky, difficult to integrate and expensive hardware, such as the system presented in the work of Oddo et al. [16]. In order to achieve cost effective and compact, light weight, solutions, it would be necessary to exploit solely the measurement already available on boards of the myoelectric prostheses, such as the EMG and motor current [18]. For example in literature it has been shown that a non-linear relationship between electromyographic signal (EMG) and generated force exists [18], [19]. Nonetheless, the estimated forces were those generated by the muscle contraction, not the ones produced by the prosthesis. On the other hand, Sadun et al. [20] demonstrated the relationship between the behavior of the motor current and the stiffness of the grasped object. Following this principle, Casini et al. [21] applied an experimental protocol for the SoftHand prosthesis based on a look up table where the sensed motor current was related to the stiffness of the different grasped objects. However, such look-up table is strongly dependent on the design of the prosthesis and in case of different mechanical or motor characteristics the acquisitions should be done all over again. A valid alternative is the model-based approach. Deng et al. [22] applied an analytical approach to estimate the object stiffness starting from the motor current for a 1 DoF system. This solution becomes particularly time-consuming when applied to a poly-articulated prosthetic hand. Among the different model-based approaches, multi-body models allow to better simulate the interaction between multi DoFs robots and complex objects, as demonstrated by Cosenza et al. [23]. The authors of this work limited their study to a 1 DoF system.

The aim of this study is to demonstrate the potentiality to exploit a multi-body approach to train object stiffness recognition algorithms for under-actuated and under-sensorized poly-articulated upper-limb prosthetic hands. For this purpose, we developed and validated a multi-body

Research was supported by INAIL, grant iHannes 2021-2024

G. Bruni, A. Bucchieri, F. Tessari, N. Boccardo, A. Marinelli, M. Laffranchi, L. De Michieli are with the Rehab Technologies Lab, Istituto Italiano di Tecnologia, Genova 16163 Italy (Tel.: 0039-010-28961; giulia.bruni@iit.it, anna.bucchieri@iit.it

A. Marinelli is also with the Department of Informatics, Bioengineering, Robotics and systems Engineering, University of Genova, 16145 Italy. A. Bucchieri and E. De Momi with the Department of Electronics, Information, and Bioengineering, Politecnico di Milano, Milan 20133, Italy elena.demomi@polimi.it

model of the Hannes [2] prosthetic hand that is able to mimic the real device both kinematically and dynamically, with the advantage of providing useful measurements otherwise not accessible (e.g. accurate estimation of frictions). The model has been experimentally validated using an external force sensor to compare the model outcomes to the actual results. By investigating the relationship between the motor current and the forces exerted by the fingers on grasped objects, we propose a novel control strategy for Hannes prosthetic hand, consisting in implementing the object stiffness recognition based on a classifier trained solely using data from the model and finally tested on the real prosthesis. This sort of model-based object stiffness recognition can represent an alternative to complex, expensive, and difficult to integrate physical force sensors.

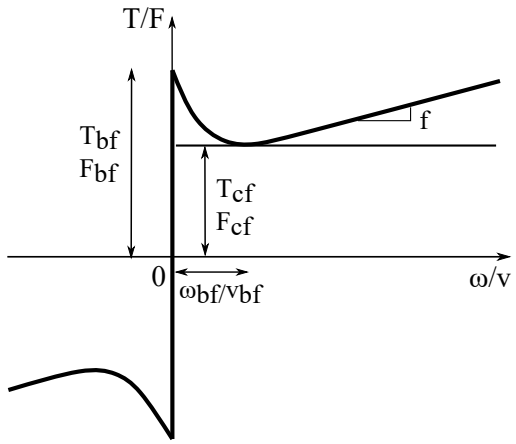

Fig. 2: Variation of friction torque/force (on the vertical axis) with respect to angular/linear velocity (on the horizontal axis).

II. MATERIALS AND METHODS

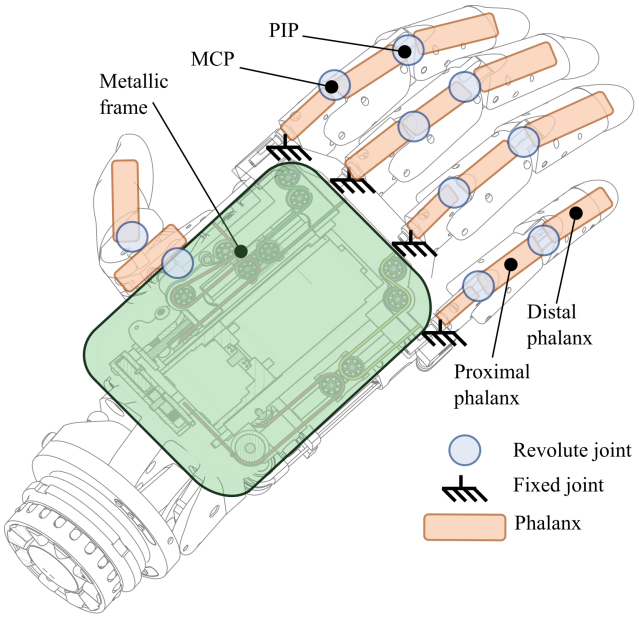

Fig. 1: Schematic representation of the main components of Hannes multi-body model: Each finger is composed by three phalanges (in orange) connected between each other by means of revolute joints (in blue). Each finger, excepted for the thumb, is connected to the metallic frame (in green) by means of a fixed joint (in black). Inside both the fingers and the metallic frame, the leader-follower system was modelled. MCP stands for metacarpophalangeal joint and PIP for proximal interphalangeal joint.

A. Hannes hand

Hannes is an under-actuated poly-articulated prosthetic hand characterized by a leader-follower wire configuration used to control the movements of fingers. The peculiarity of the prosthetic hand is the differential mechanism which makes Hannes capable of adapting to objects of any shape [2]. The follower wires are coupled with the leader system thanks to two differential systems mounted onto two linear guides, each made of custom-made bush bearing and two rails along which the bushing moves. When the linear guide is pulled down due to leader wire tension, the force acting on the follower wire generates a moment at the level of metacarpophalangeal (MCP) and proximal interphalangeal (PIP) joints [2]. The system actuation consists of a single brushed DC motor coupled with a planetary gearhead and driven by a Pulse-Width Modulation (PWM) signal generated by an input reference position. A control loop is implemented by exploiting a magnetic encoder which supplies the measured position to control unit [2].

B. Hannes multi-body model

Hannes multi-body model was created by using Simscape multi-body because of its capability of interfacing with Matlab (Mathworks) for the data post-processing. Specifically, Matlab 2020b version was used for this research. The CAD model of the Hannes hand was imported into the Simscape (Matlab 2020b) environment allowing for the correct reconstruction of all the relevant degrees of freedom offered by the prosthesis (see Fig. 1). The resulting multi-body model consisted of a series of rigid links connected by means of revolute joints (phalanxes). Subsequently, each model subcomponent (assumable as a rigid body) was characterized with the same inertial characteristics (masses and matrices of inertia) and Range of Motion (RoM) of the actual Hannes hand. The next step consisted in modeling the leader-follower system and the passive re-opening mechanism composed by pulleys and wires. In particular, once the passive components were modeled, both the power train (DC motor with 19:1 hypocycloid drive reducer) and position control (two PIDs closed-loop control strategy) were designed accordingly to the real system. Moreover, an estimation of the frictions present at both the finger joints and sliding carts levels of the differential mechanism was conducted by exploiting the theory reported in [24] where the friction torque/force profile combines both the static and viscous elements as follow:

$$T = \sqrt{2e}(T_{bf} - T_{cf})e^{-\left(\frac{\omega}{\omega_{bf}\sqrt{2}}\right)^2} \frac{\omega}{\omega_{bf}\sqrt{2}} + T_{cf}\tanh\left(\frac{\omega}{0.1\omega_{bf}}\right) + f\omega \quad (1)$$

$$F = \sqrt{2e}(F_{bf} - F_{cf})e^{-\left(\frac{v}{v_{bf}\sqrt{2}}\right)^2} \frac{v}{v_{bf}\sqrt{2}} + F_{cf}\tanh\left(\frac{v}{0.1v_{bf}}\right) + fv \quad (2)$$

Where T_{bf} stands for Breakaway Friction Torque, F_{bf} for Breakaway Friction Force, T_{cf} for Coulomb Friction Torque, F_{cf} for Coulomb Friction Force, ω_{bf}/v_{bf} for Breakaway Friction Velocity, and f for Viscous Friction Coefficient (see Fig. 2). Eq. 1 represents the friction torque in contact between rotating bodies, meanwhile Eq. 2 represents friction force in contact between moving objects. Parameters estimation reported in Table I was possible exploiting a Simulink (Matlab) optimization tool (Simulink Design Optimization™) which, starting from the motor position reference fed as input to the tool, tunes the previously mentioned static and viscous elements by minimizing the error between the simulated and real prosthesis closure time. The resulting model was finally validated both in terms of position and current measurements of the model and the real hand.

TABLE I: Order of magnitude of the estimated non-ideality at the level of joints and linear guides of the carts.

Joint	T_{bf} [Nm]	ω_{bf} [rpm]	T_{cf} [Nm]	f [Nm/(rad/s)]
MCP	10^{-2}	10^{2}	10^{-2}	10^{-3}
PIP	10^{-2}	10^{2}	10^{-3}	10^{-3}
	F_{bf} [N]	V_{bf} [mm/s]	F_{cf} [N]	f [N/(mm/s)]
Linear guide	10^{-2}	10	10^{-2}	10^{-3}

C. Object interaction

Depending on how the contact forces are modeled, the contact behavior of the two solids changes consequently. In general, the two bodies exert on each other a normal force and a friction force when in contact. These two forces were modeled using the penalty method [25]. This method attributes the normal force exchanged between the surfaces (F_n) as a function of the penetration depth of the two bodies. Specifically, the contact is modeled as a spring-damper system described by the following equation:

$$F_n = \beta\dot{x} + kx \quad (3)$$

Where β is the contact damping, and k is the contact stiffness. A higher contact stiffness will mean a smaller penetration at a given force, while the contact damping will regulate the penetration viscosity. As a consequence, the resulting F_n is based on the penetration depth (x) and the penetration velocity ($\dot{x}$). The friction force, instead, lies in the contact plane and opposes the relative tangential velocities between the two bodies near the area of penetration. In this work, we investigated the interaction between the five fingers and a hand dynamometer with the aim of experimentally

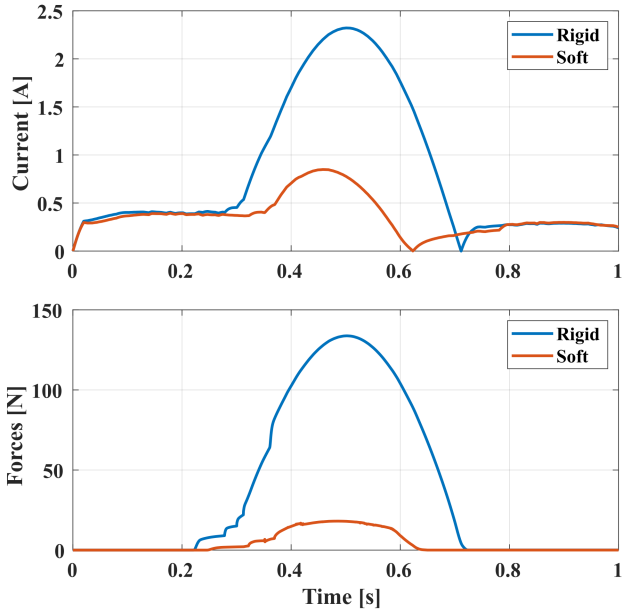

Fig. 3: (Top) The graph shows the comparison between the motor current generated by the model when interacting with a rigid object (in blue) and the one generated when interacting with a soft object (in red). (Bottom) The graph shows the comparison of the simulated grasp force in case of interaction with a rigid object (in blue) and a soft one (in red).

measure the interaction forces. The hand dynamometer was also modeled in the multi-body environment as a rigid object presenting the same geometrical characteristics of the real device. As in the real system, the sensing part was modeled on top of the simulated object. The position of the simulated object with respect to the hand was modeled as close as possible to the real set-up to minimize force estimation errors due to misalignment and have comparable experimental settings. The dynamometer contact properties (stiffness, damping and friction) were not known a priori and were tuned by minimizing the error between the simulated and the real motor current when tracking the same input command. Once matched, we compared the simulated grasping force given by the interaction force of each phalanx and the object and the one measured by the hand dynamometer. After the dynamometer validation, the developed model was used to investigate the interaction between the multi-body hand and either a rigid (the dynamometer) or soft (a ball) object. In Fig. 3 we compared both the motor currents generated by the model when interacting with the rigid (dynamometer) and the soft (ball) objects and the estimated grasp forces resulting from the interaction. It's possible to notice how the two simulated motor currents have the same behavior during void closure phase (0-0.3 seconds) and void opening phase (0.7-1 seconds), and then differentiate during the actual interaction phase (0.3-0.7 seconds) which corresponds to the interval when the modeled fingers interact with the two simulated objects. During this event one can notice how both the slopes and peak currents show substantial differences. A similar behavior is observed by comparing the generated forces during the interaction with the same two objects. Before and

after the interaction (0-0.3 seconds and 0.7-1 seconds) the forces are null, meanwhile during the grasping phase the two curves present different slopes and peak force values too. These observations highlight an existing correlation between the amplitude of motor current and the stiffness of the object.

D. Object stiffness recognition

From the above considerations, an object stiffness recognition application was implemented. The idea was to exploit the multi-body model to extract generated motor current and position following different kind of interactions in terms of objects shapes and positions. Particularly three shapes were considered (cylindrical, prismatic and spherical) with different dimensional characteristics and positions with respect to the modeled prosthetic hand. Eighteen interactions were considered of which sixteen were exploited for the training data-set and the remaining two as test data-set. The stiffnesses assigned to these objects were the ones used to model the hand dynamometer and the ball. These data were used as inputs for the training of an Ensemble bagged Tree classifier by employing the Matlab app Classification Learner. Ensemble is a supervised learning algorithm which trains a set of classifiers in parallel. Each classifier makes a prediction about the new data which is finally labelled with the prediction with the highest number of votes. The one used for our classification is the bagged trees. Bagged is the abbreviation of bootstrap aggregating and it involves that each classifier's vote has the same weight. In particular bagged trees employ the random forest algorithm which implies that the classifiers are decision trees. The decision trees are generated from a random selection of attributes at each node to determine the split [26]. The classifier was afterward tested offline on measurements acquired from the real prosthetic hand while interacting with 10 real objects of different size and stiffness (see Fig. 4) divided between rigid and soft as reported in Table III.

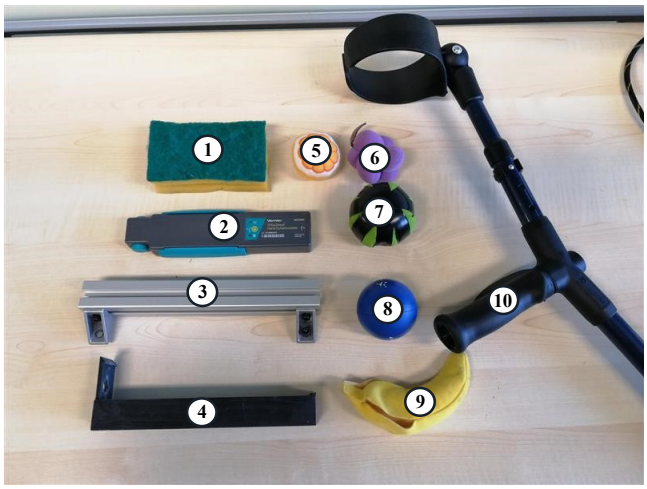

Fig. 4: The 10 objects used to test the classifier: 1) Sponge, 2) Hand dynamometer, 3) Aluminium block, 4) Ultem block, 5) Orange plush, 6) Grape plush, 7) Green ball, 8) Blue ball, 9) Banana plush, 10) Crutch handle.

E. Experimental Set-up and performance metrics

In order to verify the reliability of the computed interaction forces between the model and the hand dynamometer, an experimental set-up was built to acquire data from the real prosthesis (see Fig. 5). Firstly, the Hannes hand was directly connected to the main power supply, which guaranteed a constant voltage supply of 12 V to the electronics, this was done to avoid the introduction of further non-ideality due to battery discharge. Secondly, Hannes control board was connected to a PC through an USB cable and then controlled through a dedicated GUI (see Fig. 5). The test bench was used to acquire the grasping force. The structure consists of a custom-made system designed to support the Vernier Hand Dynamometer, composed by movable parallel arms and a two-cuffs system acting as holder. Finally, data from Hannes were acquired in a specific configuration as shown in Fig. 5. The mechanical structure of the wrist, not included in the model, was disassembled from the prosthesis and the hand was directly fixed to the test bench. Fig. 8 shows the comparison between model and Hannes data obtained while performing the same dynamometer grasping task. In particular, the average motor current during void closure and reopening, the rising and falling slope and the peak currents were compared. On the other hand, for the forces only the peak forces were considered. We employed the relative error percentage as a metric:

$$\epsilon_{\%} = \frac{V_m - V_s}{V_m} \cdot 100 \tag{4}$$

Where V_m corresponds to the value measured from Hannes, in case of the motor current estimations, and from the hand dynamometer, in case of interaction forces estimation, while V_s represents the simulated value.
The metrics used to quantitatively evaluate the classifier performance was F1Score which can be expressed as follow:

$$\text{PR} = \frac{nP}{nP + nFN}$$
$$\text{RE} = \frac{nP}{nP + nFP}$$
$$\text{F1Score} = 2 \cdot \frac{PR \cdot RE}{PR + RE} \cdot 100$$

where nP is the number of true positive, nN the number of true negative, nFP the number of false positive and nFN the number of false negative, PR is the Precision and RE the Recall.

III. RESULTS

A. Position estimation

In terms of position, the difference between the closure times of the actual Hannes hand (computed through the motor encoder signal measurement) and the multi-body model one was calculated (see Fig. 6). Results showed a negligible relative percentage error (<1%) between maximum values which overall reflects a correct estimation of the non-ideality in the model. The two curves present comparable amplitude and slope.

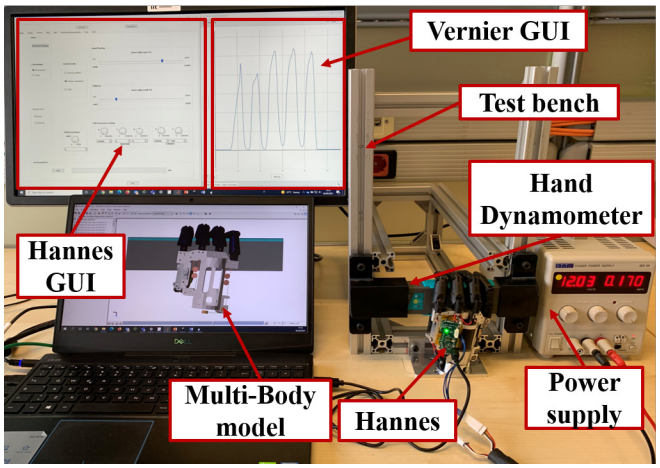

Fig. 5: Experimental set-up: On the left side of the monitor, it's possible to see the GUI through which Hannes prosthetic hand (on the right) can be controlled. On the right side of the monitor, the force measurement is shown thanks to the Vernier GUI. On the laptop the multi-body model of Hannes is shown in a Simscape environment. In the picture it's possible to see the test bench too at which the hand-dynamometer is attached by means of cuffs.

B. Motor current estimation

In terms of current, first we compared the motor current generated by the model during void closure, i.e. without any object to grasp, with the one measured by different Hannes hands presenting the same hardware and firmware version (see Fig. 7). It is possible to observe that the multi-body model presents a current behavior that reflects the Hannes average one. From a quantitative point of view, the model estimated a steady state current absorption of 0.26 A against an average of 0.25 ± 0.03 A from the four actual Hannes hands. This results in a percentage relative error of about 4%.

Afterwards, we compared the multi-body and Hannes motor currents during the interaction with the hand dynamometer. In Table II we reported the comparison between different parameters for the motor current of Hannes versus the model. Particularly, we highlighted the differences between the average motor current during void closure (I_{avgc}) and opening (I_{avgo}), the rising (I_{sc}) and falling (I_{so}) slopes and the maximum current (see Fig. 8). The maximum relative percentage error was found for the I_{so} (+36.2%), meanwhile the smaller one for I_{avgc} (-1.2%).

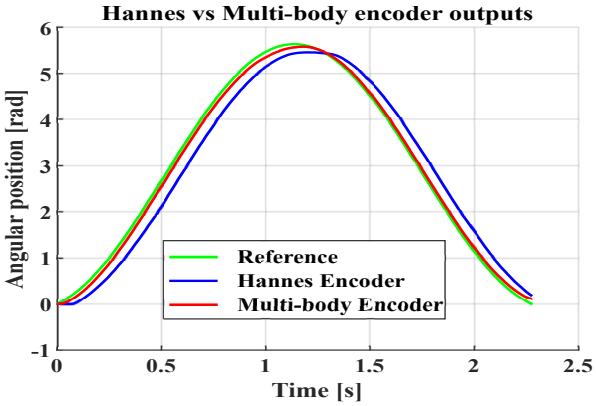

Fig. 6: Comparison between motor position reference input (in green), Hannes encoder output (in blue) and Model encoder output (in red). The relative error percentage between the closure time of Hannes and the model is <1%.

TABLE II: Parameters considered to compare the motor current of Hannes and the multi-body model. Overall the simulated hand shows a comparable behaviour with respect to the real one ($\epsilon_{\%}$ <4%), except for the opening and closing slopes ($\epsilon_{\%}$ >10%).

Test	I_{avgc}[A]	I_{avgo}[A]	I_{max}[A]	I_{sc}[A/s]	I_{so}[A/s]
Hannes	0.329	0.238	2.477	6.521	-10.577
Model	0.329	0.241	2.555	5.508	-6.749
$\epsilon_{\%}$	0%	-1.2%	-3.1%	15.5%	36.2%

C. Grasping force

The graphs in Fig. 8 shows the grasping force exerted by fingers on the dynamometer for Hannes and the multi-body model. The maximum value of the grasping force measured in Hannes reaches 194.8 N meanwhile the maximum force exerted by the multi-body model is 174.9 N, with a relative percentage error of 10.2%.

D. Classifier

Table III reports the resulting F1Scores for each tested object. The average F1Score is 91.07%. The average F1Score for rigid objects is $93.5 \pm 3.4\%$, while for soft objects is $89.5 \pm 12.5\%$.

IV. DISCUSSION

The present study aimed at investigating and exploiting the correlation between available measurements present on the Hannes prosthetic hand (i.e. motor current and position reference) and the forces exerted by the fingers on grasped objects, which are currently not quantifiable on the device. For this purpose, a multi-body model was created and validated with respect to the reference prosthesis. According to the results, both Hannes kinematics and non-ideality were correctly modeled. This is shown in Fig. 6 where

TABLE III: F1Score computation respectively for each rigid and soft object. The maximum F1Score was found during the interaction with the hand dynamometer (97.3%) and the ball (100%), meanwhile the lowest F1Score for the aluminium parallelepiped (89.3%) and the orange plush (69.5%). The total performance of the classifier resulted of 91.07%.

RIGID OBJECT	F1Score
Hand Dynamometer	97.3%
Aluminium block	89.3%
Ultem block	92.3%
Crutch handle	94.9%
SOFT OBJECT	F1Score
Blue ball	100%
Green ball	99.3%
Banana plush	88.6%
Sponge	99%
Orange plush	69.5%
Grape plush	80.53%

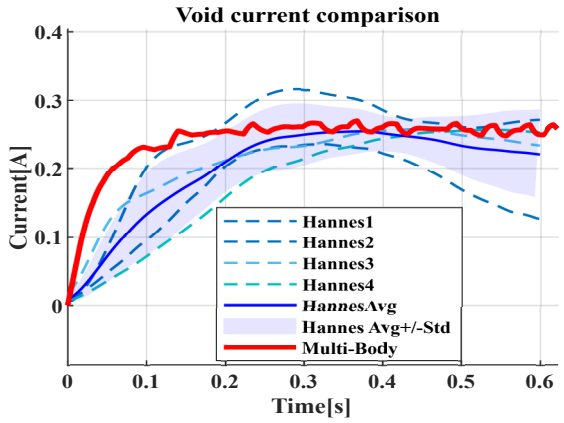

Fig. 7: Comparison between four void motor currents acquired from different Hannes hands and the model motor current. The blue dashed lines represent the four Hannes motor currents, the blue streamed line corresponds to the average between these currents, while the red streamed line is the model motor current. The blue band represents the area delimited by the average of the four currents +/- their standard deviation.

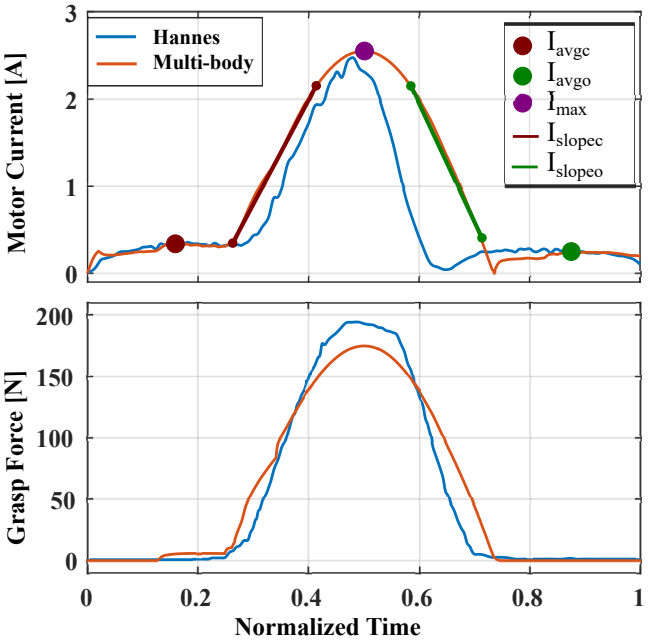

Fig. 8: The graph shows the comparison between the motor current of Hannes (in blue) and the multi-body one (in red). The two curves present a comparable behavior in terms of maximum current (I_{max}), average current during the closing (I^c_{avg}) and opening phase (I^o_{avg}). The slopes of the curves were taken into account too (I^c_{slope}, I^o_{slope}). (Bottom) The graph shows the comparison of the grasp force exerted by Hannes (in blue) on the hand dynamometer versus the simulated one (in red). In this case the two curves show a comparable behavior too.

the Hannes closing time and the model closing time are comparable (<1%). Afterwards, the simulated motor current generated by the model during a void closure was compared to different motor currents acquired directly from the real device following the same input. In Fig. 7 it's possible to observe how the slope of the red curve (Simulated motor current) during the transient phase is slightly higher than the set of blue curves (Hannes motor current). This is due to the mechanical characteristics of Hannes where the leader-follower system is characterized by a pulleys and wires system. Following consequent opening and closing of the hand, the leader wire tends to loose, thus the actuator spends the first spins to re-wind the wire on the motor pulley. Therefore, the control system is not affected immediately by the inertial components characterizing the leader-follower system and consequently the motor current rises slowly. Unfortunately, it's not possible to model the slackness of the wire in the simulation where, on the contrary, the wire is modelled as ideal and inextensible. The following step consisted in modeling and investigating the interaction of the simulated hand with virtual objects by comparing the motor currents. Fig. 8 reports the comparison between the motor current curves generated by Hannes (in blue) with respect to our model during different grasping phases (in red) of a hand dynamometer. The currents show a comparable behavior in terms of maximum amplitude and average void current during closure and opening (<4%). Instead, the error between the rising and falling slopes of the two curves is higher (>10%), probably due to the difficulty of modeling an object of unknown characteristics and recreating the same experimental conditions in the Simscape environment. Since the errors between the two motor current curves could be considered acceptable, it was possible to conclude that the stiffness of the simulated dynamometer may be close enough to the real one. Afterwards, the hand-dynamometer was used to compare the total force exerted by Hannes fingers on the object with respect to the total forces exerted by our model (see Fig. 8). The results reported an error between the maximum exerted forces around 10%. This error can be considered acceptable since for prosthetic applications it's not necessary to know the exact amplitude of the forces exerted while it's sufficient to quantify the order of magnitude to implement force control techniques. Following this, a soft object was modeled too. By comparing the behavior of both simulated motor currents and grasping forces when interacting with a rigid and a soft object, it was possible to notice a proportionality between the different stiffnesses of the objects and the current trend in terms of slope and peak amplitude. From these findings, we proposed to exploit the simulated motor current to implement an object stiffness recognition application by using a classifier. The availability of the model was a great advantage for the training of the classifier since the training set creation involves the recurrent grasp of objects which if performed with the real device would lead to the wear and damage of the mechatronic components, especially when interacting with rigid objects. To limit this type of problems, since this is an investigation phase of a new control strategy, the model was exploited. Despite being trained solely with simulated data, the classifier showed a F1Score of 91.07% when tested offline on data acquired from the real device, despite a relative high error of >10% between simulated force estimation and measured one. These results demonstrate on one hand the potentiality of this approach if implemented in real-time on Hannes hand, and on the other the reliability of the model for fast, safe and

cost-effective prototyping.

V. CONCLUSION

The presented work focused on the development of a multi-body model of an under-actuated poly-articulated prosthetic hand. The model was developed to reproduce the physical behavior of the Hannes prosthetic hand, utilizing the only available information measured on the motor side (position and current absorption of the power train) and the physical properties of the prosthesis. Sources of non-ideality, such as frictions between movable components, were estimated utilizing position and current profiles of the actual hand during opening and closure movements without object interactions. The model showed satisfactory performances with relative percentage errors below 5%. The multi-body model was experimentally validated comparing the simulated results with physical tests performed with a hand dynamometer. The comparison showed acceptable performances of the simulated hand with percentage error contained around the 10%. Once implemented and validated, the aim of this study was to exploit the simulation to find the variables currently measurable from the real device which were correlated to the stiffness of the grasped objects. The behavior of the motor current showed a proportionality with respect to the grasping force exerted by the simulated fingers on the objects, leading to the implementation of a novel control strategy involving the use of a classifier to recognize the stiffness of the grasped objects. Future developments will involve the real-time implementation of the proposed control strategy on Hannes with the aim of providing an haptic feedback to the users and improve the prosthesis embodiment.

REFERENCES

[1] D. A. Bennett, S. A. Dalley, D. Truex, and M. Goldfarb, "A multi-grasp hand prosthesis for providing precision and conformal grasps," *IEEE/ASME Transactions on Mechatronics*, vol. 20, no. 4, pp. 1697–1704, 2014.

[2] M. Laffranchi, N. Boccardo, S. Traverso, L. Lombardi, M. Canepa, A. Lince, M. Semprini, J. Saglia, A. Naceri, R. Sacchetti *et al.*, "The hannes hand prosthesis replicates the key biological properties of the human hand," *Science Robotics*, vol. 5, no. 46, 2020.

[3] S. B. Godfrey, K. D. Zhao, A. Theuer, M. G. Catalano, M. Bianchi, R. Breighner, D. Bhaskaran, R. Lennon, G. Grioli, M. Santello *et al.*, "The softhand pro: Functional evaluation of a novel, flexible, and robust myoelectric prosthesis," *PloS one*, vol. 13, no. 10, p. e0205653, 2018.

[4] M. Controzzi, F. Clemente, D. Barone, A. Ghionzoli, and C. Cipriani, "The sssa-myhand: a dexterous lightweight myoelectric hand prosthesis," *IEEE Transactions on Neural Systems and Rehabilitation Engineering*, vol. 25, no. 5, pp. 459–468, 2016.

[5] E. A. Biddiss and T. T. Chau, "Upper limb prosthesis use and abandonment: a survey of the last 25 years," *Prosthetics and orthotics international*, vol. 31, no. 3, pp. 236–257, 2007.

[6] A. Chatterjee, P. Chaubey, J. Martin, and N. Thakor, "Testing a prosthetic haptic feedback simulator with an interactive force matching task," *JPO: Journal of Prosthetics and Orthotics*, vol. 20, no. 2, pp. 27–34, 2008.

[7] R. Clement, K. E. Bugler, and C. W. Oliver, "Bionic prosthetic hands: A review of present technology and future aspirations," *The surgeon*, vol. 9, no. 6, pp. 336–340, 2011.

[8] P. E. Patterson and J. A. Katz, "Design and evaluation of a sensory feedback system that provides grasping pressure in a myoelectric hand," *J Rehabil Res Dev*, vol. 29, no. 1, pp. 1–8, 1992.

[9] C. Pylatiuk, A. Kargov, I. Gaiser, T. Werner, S. Schulz, and G. Bretthauer, "Design of a flexible fluidic actuation system for a hybrid elbow orthosis," in *2009 IEEE International Conference on Rehabilitation Robotics*. IEEE, 2009, pp. 167–171.

[10] T. Rosenbaum-Chou, W. Daly, R. Austin, P. Chaubey, and D. A. Boone, "Development and real world use of a vibratory haptic feedback system for upper-limb prosthetic users," *JPO: Journal of Prosthetics and Orthotics*, vol. 28, no. 4, pp. 136–144, 2016.

[11] B. Massa, S. Roccella, M. C. Carrozza, and P. Dario, "Design and development of an underactuated prosthetic hand," in *Proceedings 2002 IEEE international conference on robotics and automation (Cat. No. 02CH37292)*, vol. 4. IEEE, 2002, pp. 3374–3379.

[12] A. Mottard, T. Laliberté, and C. Gosselin, "Underactuated tendon-driven robotic/prosthetic hands: design issues." in *Robotics: Science and Systems*, vol. 7, 2017.

[13] G. P. Kontoudis, M. V. Liarokapis, A. G. Zisimatos, C. I. Mavrogiannis, and K. J. Kyriakopoulos, "Open-source, anthropomorphic, underactuated robot hands with a selectively lockable differential mechanism: Towards affordable prostheses," in *2015 IEEE/RSJ international conference on intelligent robots and systems (IROS)*. IEEE, 2015, pp. 5857–5862.

[14] A. Chatterjee, P. Chaubey, J. Martin, and N. Thakor, "Testing a prosthetic haptic feedback simulator with an interactive force matching task," *JPO: Journal of Prosthetics and Orthotics*, vol. 20, no. 2, pp. 27–34, 2008.

[15] M. Zandigohar, M. Han, M. Sharif, S. Y. Gunay, M. P. Furmanek, M. Yarossi, P. Bonato, C. Onal, T. Padir, D. Erdogmus *et al.*, "Multimodal fusion of emg and vision for human grasp intent inference in prosthetic hand control," *arXiv preprint arXiv:2104.03893*, 2021.

[16] C. M. Oddo, S. Raspopovic, F. Artoni, A. Mazzoni, G. Spigler, F. Petrini, F. Giambattistelli, F. Vecchio, F. Miraglia, L. Zollo *et al.*, "Intraneural stimulation elicits discrimination of textural features by artificial fingertip in intact and amputee humans," *elife*, vol. 5, p. e09148, 2016.

[17] T. Rosenbaum-Chou, W. Daly, R. Austin, P. Chaubey, and D. A. Boone, "Development and real world use of a vibratory haptic feedback system for upper-limb prosthetic users," *JPO: Journal of Prosthetics and Orthotics*, vol. 28, no. 4, pp. 136–144, 2016.

[18] J. Woods and B. Bigland-Ritchie, "Linear and non-linear surface emg/force relationships in human muscles. an anatomical/functional argument for the existence of both." *American journal of physical medicine*, vol. 62, no. 6, pp. 287–299, 1983.

[19] Y. Ban, "Estimating the direction of force applied to the grasped object using the surface emg," in *International Conference on Human Haptic Sensing and Touch Enabled Computer Applications*. Springer, 2018, pp. 226–238.

[20] A. S. Sadun, J. Jalani, and F. Jamil, "Grasping analysis for a 3-finger adaptive robot gripper," in *2016 2nd IEEE International Symposium on Robotics and Manufacturing Automation (ROMA)*. IEEE, 2016, pp. 1–6.

[21] S. Casini, M. Morvidoni, M. Bianchi, M. Catalano, G. Grioli, and A. Bicchi, "Design and realization of the cuff-clenching upper-limb force feedback wearable device for distributed mechano-tactile stimulation of normal and tangential skin forces," in *2015 IEEE/RSJ International Conference on Intelligent Robots and Systems (IROS)*. IEEE, 2015, pp. 1186–1193.

[22] H. Deng, X. Xu, W. Zhuo, and Y. Zhang, "Current-sensor-based contact stiffness detection for prosthetic hands," *IEEE Access*, vol. 8, pp. 29 456–29 466, 2020.

[23] C. Cosenza, V. Niola, and S. Savino, "A mechanical hand for prosthetic applications: multibody model and contact simulation," *Proceedings of the Institution of Mechanical Engineers, Part H: Journal of Engineering in Medicine*, vol. 232, no. 8, pp. 819–825, 2018.

[24] B. Armstrong and C. de Wit, "Canudas," friction modeling and compensation", the control handbook," 1995.

[25] J. G. De Jalon and E. Bayo, *Kinematic and dynamic simulation of multibody systems: the real-time challenge*. Springer Science & Business Media, 2012.

[26] L. Breiman, "Bagging predictors," *Machine learning*, vol. 24, no. 2, pp. 123–140, 1996.